Proceedings of the ASME 2010 Dynamic Systems and Control Conference
DSCC2010
September 12-15, 2010, Cambridge, Massachusetts, USA

DSCC2010-4085

NONLINEAR FAULT DETECTION AND ISOLATION FOR A LITHIUM-ION BATTERY MANAGEMENT SYSTEM

Jim Marcicki
Center for Automotive Research
Department of Mechanical Engineering
The Ohio State University
Columbus, OH 43212
marcicki.1@osu.edu

Simona Onori
Center for Automotive Research
The Ohio State University
Columbus, OH 43212
onori.1@osu.edu

Giorgio Rizzoni
Center for Automotive Research
Department of Mechanical Engineering
The Ohio State University
Columbus, OH 43212
rizzoni.1@osu.edu

ABSTRACT

Lithium-ion batteries are a growing source for electric power, but must be maintained within acceptable operating conditions to ensure efficiency and reliability. Therefore, a robust fault detection and isolation scheme is required that is sensitive enough to determine when sensor or actuator faults present a threat to the health of the battery. A scheme suitable for a hybrid electric vehicle battery application is presented in this work. The diagnostic problem is formulated as a nonlinear parity equation approach, but is modified for the considered application. Sliding mode observers are designed for input estimation, while the output voltage estimation is performed using an open loop model. The selection of optimal thresholds given a maximum allowable probability of error is also considered. An assessment of the design using real-world driving-cycle data leads to the conclusion that the estimation error of the observers determines a lower bound on the minimum detectable fault magnitude.

NOMENCLATURE

SOC	State of charge (0 – 1)
f_s	Fan setting (0,1,2,3)
I	Current (A)
V	Voltage (V)
T	Temperature (˚C)
r_i	Residual ($i = fs,I,V$)
mc	Battery heat capacity (kJ·˚C^{-1})
R	Battery internal resistance (Ω)
R_0C_0	Electrical time constant (s)
E_0	Open circuit voltage (V)

INTRODUCTION

Batteries continue to gain momentum as an energy storage method for vehicle propulsion applications. In particular, the number of hybrid electric vehicles (HEVs) on the road is steadily increasing because they offer superior fuel economy and reduced emissions as compared to conventional vehicles. In order to ensure efficient, reliable operation of the battery pack, it must be regulated to an acceptable range of operating conditions. For instance, operation at low SOC or high temperatures will significantly shorten the life of the battery. In addition, battery failure due to thermal runaway has the potential to cause injuries to vehicle passengers. Therefore, battery systems must be designed to maintain safe and efficient operation [1], which requires online estimation of a number of battery properties. In turn, accurate estimation requires definitive knowledge of whether sensor faults are present, a problem which is often neglected when designing battery management algorithms [1-3]. This paper is concerned with fault detection and isolation (FDI) within the battery management system of a representative HEV Lithium-ion (Li-ion) battery pack. A high-level schematic of the considered system is shown in Fig. 1.

In a system with this level of sophistication, and therefore complexity, there are several places where faults may adversely affect performance. This fact drives the need for a (FDI) system whose key objectives may be summarized as follows:

- use available measurements to determine faulty components;
- minimize the probability of error, both from false alarms and missed detections;
- pass fault information to the control system to enable fault tolerant control.

Of these three main objectives, the first two are considered in the design of the FDI scheme presented in this paper. The last objective is considered outside the scope of this work, though it motivates many of the presented results.

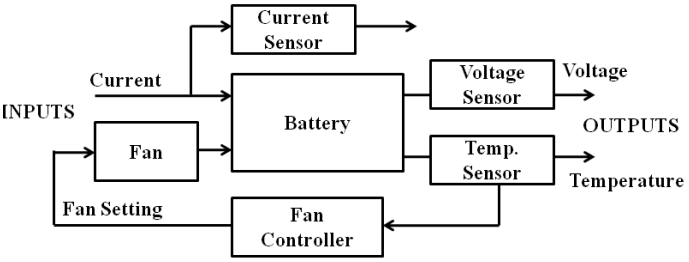

FIGURE 1. SCHEMATIC OF BATTERY SYSTEM SHOWING SYSTEM INPUTS AND OUTPUTS.

In order to aid in the design of FDI schemes, a nonlinear electro-thermal battery model has been developed. This model is presented in the next section, along with an introduction to the fault modes. Then, the FDI strategy is discussed. A number of nonlinear FDI methods are surveyed in [4]. The nonlinear parity equation residual generation (NPERG) scheme [5] is chosen for this study because it is general enough to diagnose many permutations of faults. This arises from the limitless number of faults that may be hypothesized, though the complexity of the scheme obviously increases as well. NPERG has been used effectively in internal combustion engine and chassis system FDI [6-7] and due to its versatility it may also be applied to battery systems. A modified method is proposed specifically for the model structure presented here. The design of the observers and thresholds is detailed thereafter. Finally the results, conclusions, and areas of future work are discussed.

MODEL DEVELOPMENT

Here the equations that constitute the electro-thermal battery model [8] are presented. We use an equivalent circuit model structure that has been experimentally validated for a number of battery chemistries, including the Li-ion chemistry considered here. The first-order equivalent circuit model has parameters scheduled based on state-of-charge (SOC), temperature, and current direction. This model captures the dominant transient processes that are neglected by a zero-order model, while avoiding the computational and calibration complexity of higher-order lumped or first-principle based models. The model structure may be divided into three coupled sub-models, namely the electric, thermal, and state-of-charge dynamics.

Electric Dynamics. Figure 2 depicts the electric model framework. The simple first-order model is able to adequately compute the voltage-current relationship of the battery over a wide range of operating conditions due to the scheduling of the open circuit voltage (OCV) E_0, internal resistances R and R_0, and capacitance C_0.

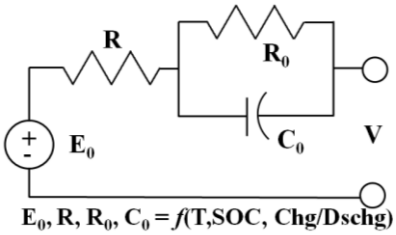

FIGURE 2. FIRST-ORDER EQUIVALENT CIRCUIT MODEL OF BATTERY ELECTRIC DYNAMICS.

The electrical model equations obtained using Kirchoff's current law are reported in Eq. 1 and Eq. 2.

$$\dot{V}_c = \frac{-1}{R_0 C_0} V_c + \frac{1}{C_0} I \qquad (1)$$

$$V = E_0 - IR - V_c \qquad (2)$$

The input to the electric sub-system is the current, I, and the output of the sub-system is the battery terminal voltage, V. The state of the sub-system is the voltage across the capacitor, V_c. Note that in this model the total pack voltage is obtained by scaling a single cell voltage by the number of cells.

Thermal Dynamics. The battery is modeled as a lumped thermal mass with uniform temperature T throughout the entire pack. We understand more detailed thermal models such as those discussed in [9] could be applied here, and validation of the current methodology with such a model may become an area of future work. Nevertheless, the thermal sub-system consists of the energy balance in Eq. 3.

$$mc\dot{T} = RI^2 - hA(T - T_\infty) \qquad (3)$$

The effective heat capacity mc and the ambient temperature T_∞ are fixed constants. The energy balance accounts for heat generation due to Joule heating and heat dissipation from convection. It has been assumed that the internal resistance R is solely responsible for Joule heat generation. This assumption is

supported by calculations showing it accounts for at least 90% of the total heat generation for the current profiles considered here. It is important to note that the effective heat transfer coefficient hA varies depending on the type of convection. A fan is incorporated into the system to increase the rate of cooling during times when the temperature rises above specific thresholds. It modifies the effective heat transfer coefficient in the manner of Eq. 4.

$$hA = hA_0(1+fs),\ fs = 0,1,2,3 \qquad (4)$$

In Eq. 4, hA_0 is the natural convection heat transfer coefficient. Table I summarizes the range of values for the fan setting fs determined via temperature based threshold control.

TABLE I. FAN CONTROL THRESHOLD SETTINGS

Setting	fs	Range (°C)
Off	0	T < 30
Low	1	30 ≤ T < 35
Medium	2	35 ≤ T < 40
High	3	T ≥ 40

In summary, the inputs to the thermal sub-system are the current, I, and the fan setting, fs. The output and state of the sub-system is the lumped battery temperature, T.

State of Charge Dynamics.: The SOC dynamics are determined simply by setting the rate of change of SOC equal to the current as in Eq. 5. It is scaled by the total capacity of the pack, Ah, and is negative for a positive (discharge) current.

$$\dot{SOC} = -I / Ah \qquad (5)$$

Parameter Scheduling. The internal resistance, OCV, and capacity of batteries are influenced by a number of factors including SOC, temperature, and current direction. The parameters of the equivalent circuit model must approximate this dependency. For example, Fig. 3 from [8] shows a representative temperature-SOC-resistance relationship.

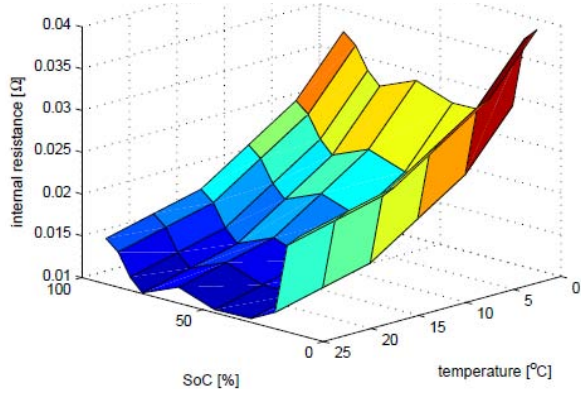

FIGURE 3. FIT OF RESISTANCE VERSUS TEMPERATURE AND SOC DATA [8].

Finally, Fig. 4 summarizes the relationship between the described sub-models graphically.

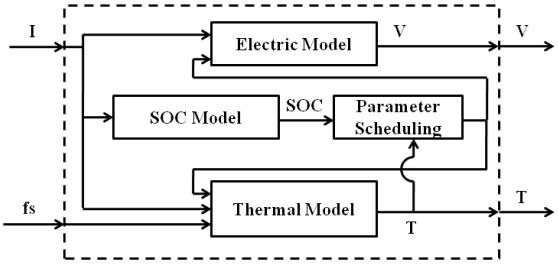

FIGURE 4. RELATIONSHIP BETWEEN SUB-MODELS.

Considered Faults

In a typical industrial scenario, a hazard analysis would be the first step towards characterizing the location and severity of possible faults. In this work it is assumed that a suitable hazard analysis has been performed, and that the most interesting potentially faulty components are the current, voltage, and temperature sensors, and the fan motor.

Based on operational experience at the Center for Automotive Research (CAR) [10], we have defined methods for realistic fault injection. The two types of sensor faults that are considered in this work are intermittent signal loss due to faulty wiring connections, and sensor bias resulting from time or temperature drift. For the fan motor, the only fault that is considered is a total motor failure where it can no longer provide cooling to the battery.

FDI STRATEGY AND DESIGN

In this section, the applicability of the NPERG method is discussed for the battery management system. Through definition of the estimation error dynamics, it is shown that a modified approach is required. Such an approach is pursued at the expense of complete isolation of faults after they are detected.

NPERG Method

The NPERG method is a general approach to the design of fault detection algorithms for non-linear systems, and so it is used as a starting point here. The methodology states that a subset of inputs and outputs are hypothesized to be non-faulty, and residuals are generated based on this assumption. Residuals are defined as the difference between the estimated and actual values of a signal, and computing these differences requires both forward and inverse models of the system. One important point is that the inverse model of the system only needs to invert the subsystem of interest, which can have a dimension less than the complete system. Detection and isolation of faults is achieved based on the hypothesized non-faulty subset of inputs and outputs and the signature of the residuals. The process is shown graphically in Fig. 5 on the next page. The first residual generator assumes voltage and fan setting are non-faulty. An inverse model is used to

calculate the input current, which is then used as the input to a forward model that computes the battery temperature residual.

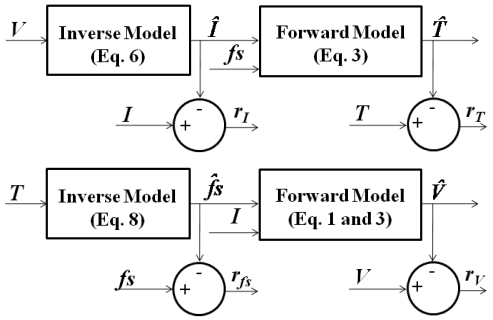

FIGURE 5. SCHEMATIC OF NPERG FDI SCHEME.

Alternatively, the second residual generator assumes temperature and current are non-faulty and produces residuals for the fan setting and voltage sensors. Many techniques are available to design an inverse model, such as a sliding mode observer, unknown input observer, or an empirical correlation using system identification techniques. The forward model is simply a copy of the plant dynamics.

Observer Design. Due to the presence of nonlinearities in the system and its robustness to modeling errors, sliding mode observers are designed for the inverse model problem. Consider Eq. 1 with the input replaced by a discontinuous term, μ_I, as shown in Eq. 6.

$$\dot{\hat{V}}_c = -\frac{1}{R_0 C_0}\hat{V}_c + \mu_I \tag{6}$$

Then, one could define error dynamics as in Eq. 7,

$$\begin{aligned} \dot{e}_V &= -R(\dot{I} - \dot{\hat{I}}) - (\dot{V}_c - \dot{\hat{V}}_c) \\ \dot{e}_V &= \frac{1}{R_0 C_0}(V_c - \hat{V}_c) - R(\dot{I} - \dot{\hat{I}}) - \frac{I}{C_0} + \mu_I \end{aligned} \tag{7}$$

where the error is defined as $e_V = V - \hat{V}$. The error must be defined in terms of the battery terminal voltage, since the equivalent circuit capacitor voltage is not measurable. This is a mathematical representation of the inverse model from voltage to current in Fig. 5.

This expression is intractable because it contains the derivatives of the input current and the estimated input current. Additionally, the capacitor voltage enters the expression and this quantity is not an available measurement. One could proceed with this design, and choose μ_I such that it is greater than some approximation of the other terms. Upon extraction of the equivalent control term through filtering, however, these terms will remain and corrupt the current estimate. Therefore, an alternative scheme is proposed below, so that the input current may be calculated from known quantities.

Proposed Residual Generation Method

Since temperature is the only explicitly measured model state, it is preferable to use it as the input to both inverse models as in Fig. 6. In this scheme we have removed the forward model for temperature resulting in the requirement that the temperature measurement be non-faulty, which was not previously necessary.

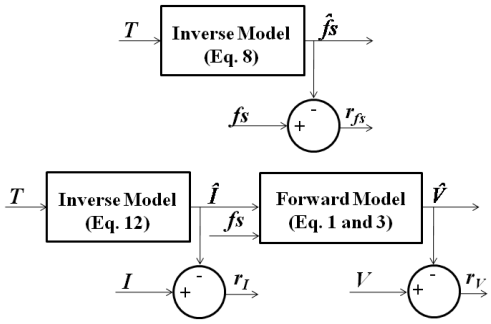

FIGURE 6. SCHEMATIC OF PROPOSED FDI SCHEME.

Observer Design. There are two inverse models required to compute estimates of the inputs using the temperature signal. The inverse model computing the fan setting from battery temperature may be defined as follows. First, the estimated temperature dynamics are given by Eq. 8, where the heat sink term due to fan cooling is replaced by μ_{fs}.

$$\dot{\hat{T}} = \frac{I^2 R}{mc} + \mu_{fs} \tag{8}$$

Next, the error dynamics of this estimate may be defined as in Eq. 9, where the error is defined as $e_{fs} = T - \hat{T}$.

$$\dot{e}_{fs} = \frac{(1+fs)hA(T - T_\infty)}{mc} - \mu_{fs} \tag{9}$$

By setting $\mu_{fs} = K_f sgn(e)$ the origin of the error ($e_{fs} = 0$) for the inverse path from temperature to fan setting is guaranteed to be asymptotically stable as long as Eq. 10 is satisfied.

$$K_f > \frac{(1+fs)hA(T - T_\infty)}{mc} \tag{10}$$

Since asymptotic stability is guaranteed, it is clear that $\dot{e}_{fs}$ will also converge to zero. Then, Eq. 11 holds if a low-pass filter is applied to μ_{fs} to extract its low-frequency content.

$$\mu_{fs} = \frac{(1+fs)hA(T - T_\infty)}{mc} \qquad (11)$$

Now the second inverse model estimating battery current from temperature must be defined. A form similar to Eq. 8 is used to obtain Eq. 12 below, where instead the heat source due to Joule heating is modeled using a discontinuous term.

$$\dot{\hat{T}} = \mu_I + \frac{(1+fs)hA(T - T_\infty)}{mc} \qquad (12)$$

Again, defining the error $e_I = T - \hat{T}$ gives the error dynamics shown in Eq. 13.

$$\dot{e}_I = I^2 R - \mu_I \qquad (13)$$

Then by setting $\mu_I = K_I sgn(T-T_\infty)$, the origin of the error dynamics for the inverse path from temperature to current are asymptotically stable when the constraint given by Eq. 14 is met.

$$K_I > \frac{I^2 R}{mc} \qquad (14)$$

After a finite length of time, e_I and $\dot{e}$ converge to zero. Application of a low-pass filter results in the equality of Eq. 15.

$$\mu_I = \frac{I^2 R}{mc} \qquad (15)$$

Finally, the forward model estimate of battery terminal voltage is given by Eq. 1, where instead of the actual current, the estimated current of Eq. 15 is defined as the input to the system. It should be noted that the modification for discrete time systems presented in [11] is used to produce the simulation results.

Fault Signature Development. Generally, fault signatures may be developed analytically for simple systems or if there is no coupling between sub-systems. However, Eqns. 1 and 3 exhibit numerous forms of coupling that make it difficult to determine the exact effects of faults. It is clear that a fault in one location of the system may produce multiple non-zero residuals. Thus, simulation is used to develop the fault signature for this system. Faults are injected, one at a time, into each of the three sensors and fan motor. In order to simplify the process of identifying the faulty response of each residual, a constant current profile is considered, but this should not change the resulting signatures for more complex inputs. The faults consist of intermittent signal losses, or in the case of the fan motor a complete loss of cooling that is non-recoverable. The simulated 'measured' values for the current, fan setting, and the output voltage of a single cell are shown in Fig. 7 along with the estimated values. The residual corresponding to each sensor is the difference between the estimated and actual values.

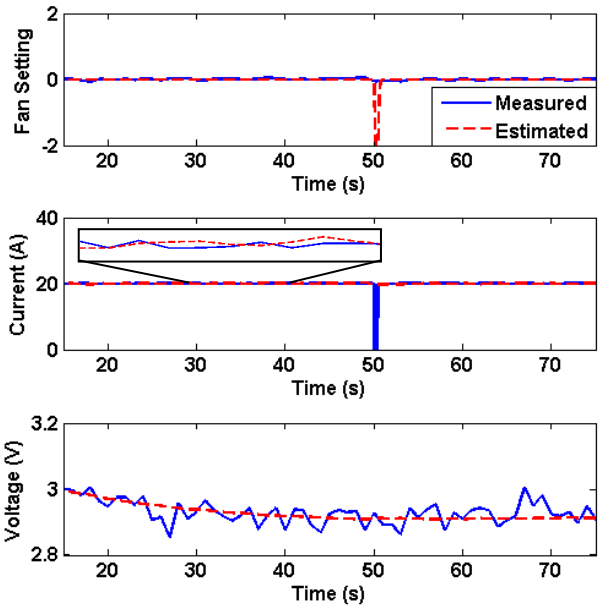

FIGURE 7. RESPONSE OF RESIDUALS TO INTERMITTENT CURRENT SENSOR FAULT AT A TIME OF 50 S.

Note that in Fig. 7, there is no distinguishable difference between the voltage estimate and the sensor value, while the fan setting and current estimates exhibit sharp differences from their measured values at the time of the fault. This process of studying the effect of faults on the residuals of the system may be repeated for faults originating in the temperature sensor, voltage sensor, and fan motor to produce a full set of fault signatures. The fault signatures resulting from the complete analysis are summarized in Table II. Isolation between the fan input and temperature sensor has not been achieved, which is a consequence of using the temperature sensor as an input to both residual generators.

Threshold Selection. Once the response of each residual to all considered faults is understood, the next step is to select thresholds for the residuals that are used to determine the presence of faults. If the residual value in question exceeds its threshold, then a sensor fault is recorded. Theoretically, the probability of error when declaring the presence of a fault may be minimized by studying the probability density function (PDF) of faulty and non-faulty signals. These functions must be obtained through extensive experimental data collection or simulation of the system. The operating conditions under which the PDF is obtained must be similar to the actual operating conditions expected for the system, to ensure that the characterization of the residuals during testing is appropriate for the intended application. For the HEV battery management system presented here, real HEV driving data obtained from [12] will be used to develop the necessary PDFs. The current profile corresponding to this data is shown in Fig. 8. In addition to using a realistic current profile, Gaussian sensor

noise is added to the model. This represents the inability to obtain exact, clean measurements during system operation and generally results in an increase in the mean square estimation error.

TABLE II. FAULT SIGNATURE SUMMARY. A VALUE OF 1 INDICATES A NON-ZERO RESIDUAL.

Fault Location	Residual	Value
T	r_I	1
	r_{fs}	1
	r_V	1
V	r_I	0
	r_{fs}	0
	r_V	1
fs	r_I	1
	r_{fs}	1
	r_V	1
I	r_I	1
	r_{fs}	1
	r_V	0

For the signal loss faults that were used to develop the fault signatures, the selection of thresholds is trivial as long as the non-faulty signal values are large enough. Logically, if the non-faulty signal values were already zero or very close to it, then the fault will not be noticed. Thus, the signal loss thresholds are set to the same value used for determining drift faults.

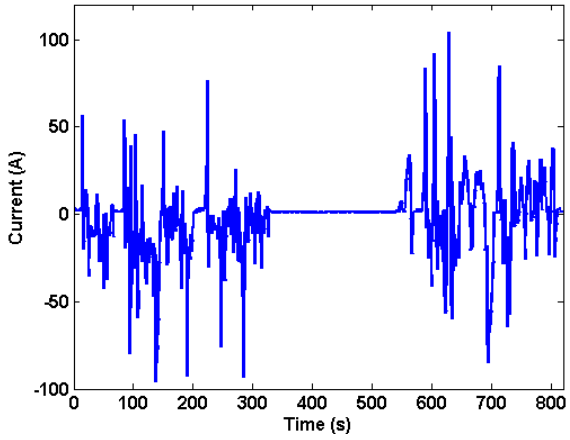

FIGURE 8. CURRENT INPUT FOR PDF DEVELOPMENT.

The selection of thresholds for detection of sensor bias faults is much more complex due to smaller fault magnitudes which result in less differentiation between faulty and non-faulty residuals. Thus, the faulty and non-faulty PDFs may have significant overlap if the variance of the residual is large relative to the bias. This is shown graphically in Fig. 9, which contains two distinct faults simulated with the current profile of Fig. 8. The top case considers the response of the current residual to a current sensor fault, while the lower case considers the response of the voltage residual to a voltage sensor fault.

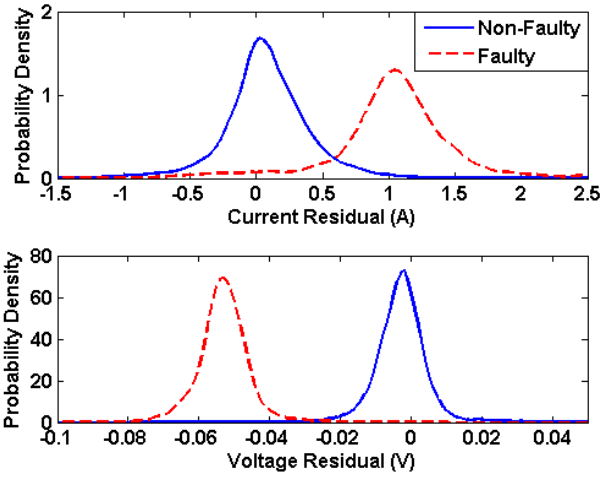

FIGURE 9. PDFs OF VOLTAGE AND CURRENT SENSOR RESIDUALS. VOLTAGE FAULT IS A -50 mV SENSOR BIAS WHILE CURRENT FAULT IS A 1 A SENSOR BIAS.

Due to the inevitable overlap of PDFs, an optimal threshold must be determined using hypothesis testing. The objective of the optimal threshold selection is to minimize the probability of error when declaring a residual faulty, or deciding a non-zero residual is too low to detect a fault. This statement is summarized by Eq. 16, where the assumption that a sensor may be faulty (H_1) or non-faulty (H_0) with equal probability has been made.

$$f_r(r \mid H_1) \underset{\hat{H}=H_0}{\overset{\hat{H}=H_1}{\gtrless}} f_r(r \mid H_0) \qquad (16)$$

The expression in simple terms states that the optimal threshold should be placed at the intersection of the PDFs. This finding comes from the desire to select the more probable hypothesis at any residual value, which is represented by the larger probability density value. Overlapped regions of the PDF, however, result in a certain probability of error either from false alarms or missed detections. This error is calculated by computing the integral of the overlapped region of the PDF. Given a nominal PDF and a maximum allowable probability of error, the amount of sensor bias (shift of residual mean) that is detectable using this method can be calculated.

RESULTS

Here the minimum detectable fault magnitudes are presented, along with simulations showing the actions of faults during a driving cycle obtained from operational HEV data.

Minimum Detectable Faults

The minimum fault magnitudes to achieve five percent or less detection error are shown in Table III.

TABLE III. MINIMUM DETECTABLE SENSOR BIAS.

Fault Location	Min. Magnitude
Current Sensor	1.2 A
Voltage Sensor	22 mV

It is clear from the above values that realistic sensor drift cannot be diagnosed without significant false alarm error, due to the large minimum fault magnitudes. For instance, we may relate the voltage sensor error to an SOC error by calculating the derivative of SOC with respect to OCV based on curves from [8]. A quick calculation gives a range of SOC error from 7% - 100% for 30-80% SOC, which is clearly too large. This problem arises because the OCV curve plateaus in the SOC range of interest. Recall that the minimum fault magnitudes are computed for a dynamic current profile; the estimation error could be improved for a designed diagnostic test with a constant discharge current.

As a possible explanation for the poor estimator performance consider that the current estimator uses temperature, which has a large time constant, as an input. Thus some of the dynamics of the original current signal are lost and a minimum bound of estimation error is present. The minimum magnitude of temperature fault is not discussed because the temperature sensor is considered faulty whenever both the current and voltage thresholds are exceeded. This implicitly assumes that a fault in a single sensor is more probable than simultaneous faults in two distinct sensors. Additionally, the fan setting threshold is simply fixed at 0.5 because it will only take discrete values with the assumption of the fault occurring as complete cooling failure.

Driving Cycle Simulations with Faults

The thresholds presented in the previous section are tested for the real-world driving cycle. The response of the system to a fan motor failure at t = 200 seconds is shown in Fig. 10. Since the loss of the cooling fan has a large impact on the system, the effects of the failure can be seen in all three residuals. To reduce the error present in the residuals of Fig. 11 from both sensor noise and sliding mode chattering, a 0.5 second moving-average is applied.

Next, the computed thresholds are tested for the case of signal loss faults. Current sensor signal loss occurs at times of 140 and 150 seconds, while voltage sensor loss occurs at times of 160 and 170 seconds. The estimation results are shown in Fig. 12, while the smoothed residuals are shown in Fig. 13.

Temperature signal loss is not considered, because it is required for convergence of the estimators. Of particular interest in the results is that there are no missed detections using these thresholds. However, there are brief false alarms in the voltage and current residuals in both cases which can generally be rejected through logical algorithms to avoid increasing the thresholds. This type of empirical tuning is typical of practical FDI.

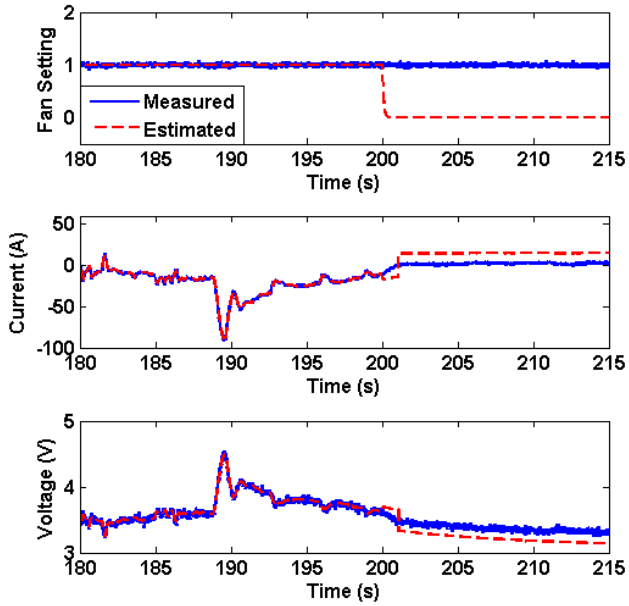

FIG. 10. FAN MOTOR FAILURE AT t = 200 SECONDS.

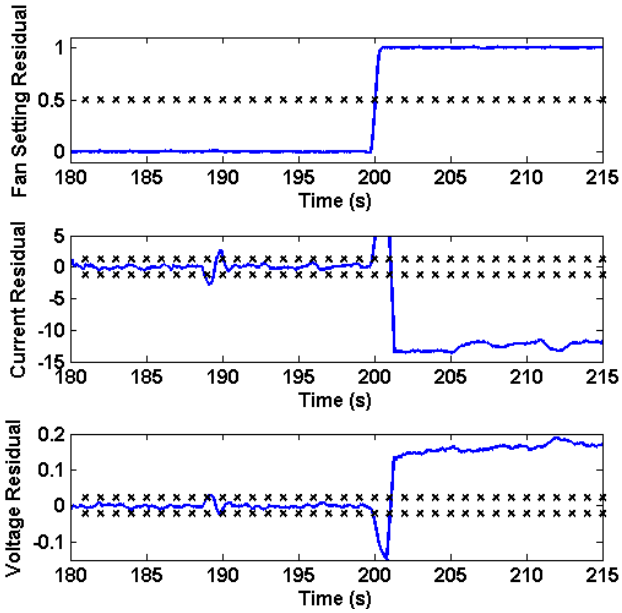

FIG. 11. RESIDUAL RESPONSES TO FAN FAULT AT t = 200 SECONDS. THRESHOLDS ARE DENOTED BY X'S.

CONCLUSIONS AND FUTURE WORK

A FDI scheme has been designed for a Li-ion HEV battery management system. The development of the system requires careful consideration of the model structure, in order to design observers whose error dynamics can be manipulated advantageously. While larger faults are easily detected by the FDI

system, useful estimates of sensor bias escape detection. This is due to the intuitive constraint that faults smaller than the normal estimation error of the observers cannot be detected, but could be corrected by employing a constant discharge diagnostic test.

Future work on this topic could include application specific rules that eliminate false alarms through the use of outlier rejection algorithms. This type of empirical adjustment would allow detection of smaller faults while still limiting false alarms. Finally, the FDI algorithm may be combined with parameter estimation to distinguish between sensor faults and natural changes that occur within the battery during aging. Robustness with respect to battery state of health is crucial for practical applications, and characterization of battery aging under a diverse range of conditions is ongoing at CAR. Incorporation of aging mechanisms into a FDI algorithm, however, would require a very accurate model of the aging process which is not a trivial task.

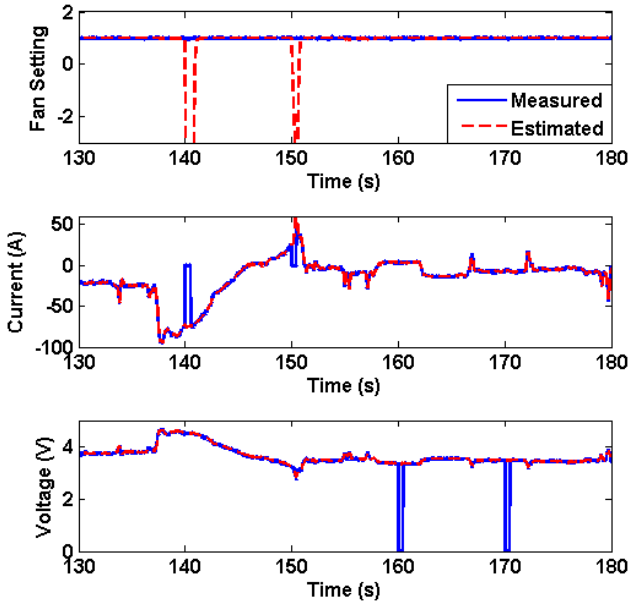

FIG. 12. INTERMITTENT VOLTAGE AND CURRENT SIGNAL LOSSES THROUGHOUT DRIVING CYCLE.

REFERENCES

[1] Chatzakis, J., Kalaitakis, K., Voulgaris, N. C., and Manias, S. N., 2003, "Designing a New Generalized Battery Management System," IEEE Transactions on Industrial Electronics, 50(5).

[2] Plett, G., 2004, "Extended Kalman filtering for battery management systems of LiPB-based HEV battery packs, Part 1: Background," Journal of Power Sources, 134, pp. 252-261.

[3] Piller, S., Perrin, M., and Jossen, A., 2001, "Methods for state-of-charge determination and their applications," Journal of Power Sources, 96, pp. 113-120.

[4] Garcia, E., and Frank, P.M., 1997, "Deterministic nonlinear observer-based approaches to fault diagnosis: A survey," Control Eng. Practice, Vol. 5, Issue 5, pp. 663-670.

[5] Krishnaswami, V., and Rizzoni, G., 1994, "Nonlinear parity equation residual generation for fault detection and isolation," Proceedings of the IFAC SAFEPROCESS '94, pp. 317–322 Espoo, Finland.

[6] Krishnaswami, V., Luh, G., and Rizzoni, G., 1995, "Nonlinear parity equation based residual generation for diagnosis of automotive engine faults," Control Engineering Practice, 3(10), pp. 1385-1392.

[7] Pisu, P., Soliman, A., and Rizzoni, G., 2003, "Vehicle Chassis Monitoring System," Control Engineering Practice, 11(3), pp. 345 – 354.

[8] Hu, Y., Yurkovich, B.J., Yurkovich, S., and Guezennec, Y., 2009, "Electro-Thermal Battery Modeling and Identification for Automotive Applications," Proceedings of the 2nd Annual ASME Dynamic Systems and Control Conference, Hollywood, CA.

[9] Muratori, M., Canova, M., Guezennec, Y., and Rizzoni, G., 2010, "A Reduced-Order Model for the Thermal Dynamics of Li-ion Battery Cells," Proceedings of the IFAC Symposium Advances in Automotive Control, Munich, Germany.

[10] Communications with John Neal, Research Engineer at OSU Center for Automotive Research. neal.166@osu.edu

[11] Utkin, V., Guldner, J., Shi, J., 1999, *Sliding Mode Control in Electromechanical Systems*. Taylor and Francis, Philadelphia, PA, pp 162, Ch. 9.

[12] OSU Center for Automotive Research operational data of demonstration plug-in hybrid. http://car.osu.edu

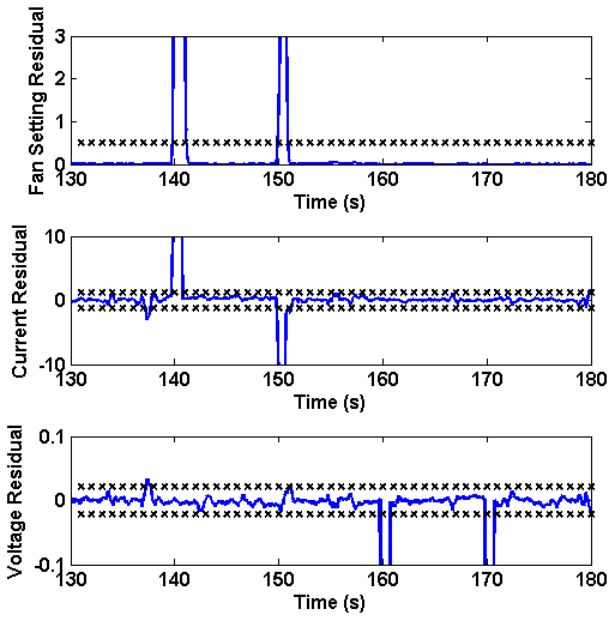

FIG. 13. RESIDUAL RESPONSES DUE TO SIGNAL LOSS FAULTS. THRESHOLDS ARE DENOTED BY X'S.